Invited Paper

Hair-based sensors for micro-autonomous systems

Mahdi M. Sadeghi, Rebecca L. Peterson and Khalil Najafi*
Center for Wireless Integrated MicroSensing and Systems (WIMS^2), University of Michigan
Ann Arbor, MI USA 48109-2122

ABSTRACT

We seek to harness microelectromechanical systems (MEMS) technologies to build biomimetic devices for low-power, high-performance, robust sensors and actuators on micro-autonomous robot platforms. Hair is used abundantly in nature for a variety of functions including balance and inertial sensing, flow sensing and aerodynamic (air foil) control, tactile and touch sensing, insulation and temperature control, particle filtering, and gas/chemical sensing. Biological hairs, which are typically characterized by large surface/volume ratios and mechanical amplification of movement, can be distributed in large numbers over large areas providing unprecedented sensitivity, redundancy, and stability (robustness). Local neural transduction allows for space- and power-efficient signal processing. Moreover by varying the hair structure and transduction mechanism, the basic hair form can be used for a wide diversity of functions. In this paper, by exploiting a novel wafer-level, bubble-free liquid encapsulation technology, we make arrays of micro-hydraulic cells capable of electrostatic actuation and hydraulic amplification, which enables high force/high deflection actuation and extremely sensitive detection (sensing) at low power. By attachment of cilia (hair) to the micro-hydraulic cell, air flow sensors with excellent sensitivity (< few cm/s) and dynamic range (> 10 m/s) have been built. A second-generation design has significantly reduced the sensor response time while maintaining sensitivity of about 2 cm/s and dynamic range of more than 15 m/s. These sensors can be used for dynamic flight control of flying robots or for situational awareness in surveillance applications. The core biomimetic technologies developed are applicable to a broad range of sensors and actuators.

Keywords: micro electro mechanical systems (MEMS), micro-hydraulics, biomimetic sensors and actuators, air flow sensor

1. INTRODUCTION

Micro-autonomous systems such as those developed under the Army Research Laboratory's MAST (Micro Autonomous Systems & Technology) program need sensory systems for dynamic robot control, mapping and navigation, and situational awareness. These platforms usually have very limited payload capacity making off-the-shelf components challenging or impossible to integrate. For some applications such as directional air flow or wind-gust detection there are no commercial parts available even if size and weight constraints are relaxed. This motivates us to investigate a new class of sensors that can offer high speed, small size, high resolution, low power and wide dynamic range. These sensors are inspired by biological hair which is characterized by arrays of high aspect ratio, three-dimensional structures, with mechanical amplification of movement and local neural (i.e., electronic) integration.

Previously there have been a few investigations into bio-mimetic hair-like air flow sensors which have established that such architectures can offer high accuracy and high resolution flow measurement[1,2]. Since the tall hair structure is oriented out of the substrate plane, a small sensor footprint is possible, enabling sensor arrays which provide redundancy and fault tolerance. Hairs with piezoresistive or capacitive transduction for air flow sensing have very fragile structures with exposed delicate electronic elements which limit their use[1,2]. These designs also exhibit a trade-off between high accuracy and large dynamic range. For instance, for a conventional capacitive sensor, a narrow capacitive gap is needed to make the device sensitive to small plate deflections and thus obtain high sensitivity[1,3]. However narrow gaps deteriorate the available sensor range. Here we exploit a micro-hydraulic structure to expand the measurement range while maintaining the same sensitivity[4,5]. The hydraulically-assisted capacitive sensor structure is shown in Figure 1. A large gap can be used on the front side to allow large range while a narrow back-side gap is used to obtain high sensitivity. Due to the asymmetric nature of micro-hydraulic system, a larger capacitive plate area on the back side can compensate for the smaller deflection on this side. In addition, since both gaps are filled with liquid and enclosed, the

*najafi@umich.edu, phone +1-734-763-6650, fax +1-734-763-9324

Micro- and Nanotechnology Sensors, Systems, and Applications IV, edited by
Thomas George, M. Saif Islam, Achyut Dutta, Proc. of SPIE Vol. 8373, 83731L

system is robust and less prone to damage in wet, windy or dusty environments compared to capacitive sensors with exposed gaps or piezoresistive sensors with narrow and fragile cantilever beams. Moreover, since capacitive transduction is a passive measurement technique, it will consume very low power compared to hair-like hot wire anemometers[6] or other thermal sensors[3,7,8] where there is a sensing element that must be heated, actively consuming power.

The sensor presented in this paper build on an earlier generation of micro-hydraulic based hair air flow sensors[9]. The device architecture and geometry have been optimized for higher bandwidth while the high sensitivity and large dynamic range are maintained. The sensor response time is mainly constrained by fluidic resistance of the encapsulated liquid. We have analyzed the dynamics of the micro-hydraulic system and determined the critical components contributing to the fluidic resistance and have co-optimized the sensor bandwidth, sensitivity and range. The fabricated sensors are found to have a fast, linear response to air flow over a large dynamic range.

2. DEVICE DESCRIPTION

2.1. Micro-hydraulic system

The basic structure of a micro-hydraulic system is shown in Figure 1. It consists of two trenches on the front and back side of a silicon wafer connected by a channel. Both trenches and the channel are filled with a silicone fluid and the trenches are capped by a 1-2 µm thick layer of Parylene to enclose the micro-hydraulic system. Either chamber can be compressed by applying pressure to the flexible Parylene membrane on one side, thus forcing the liquid into the other chamber, causing its membrane to deflect.

With a proper choice of the area ratio between the chambers, amplification of either force or displacement is achievable. This amplification, which is characteristic of the micro-hydraulic system, plays an essential role in improving sensor performance. A pair of electrodes on the back side can be used for electrostatic actuation or capacitive sensing.

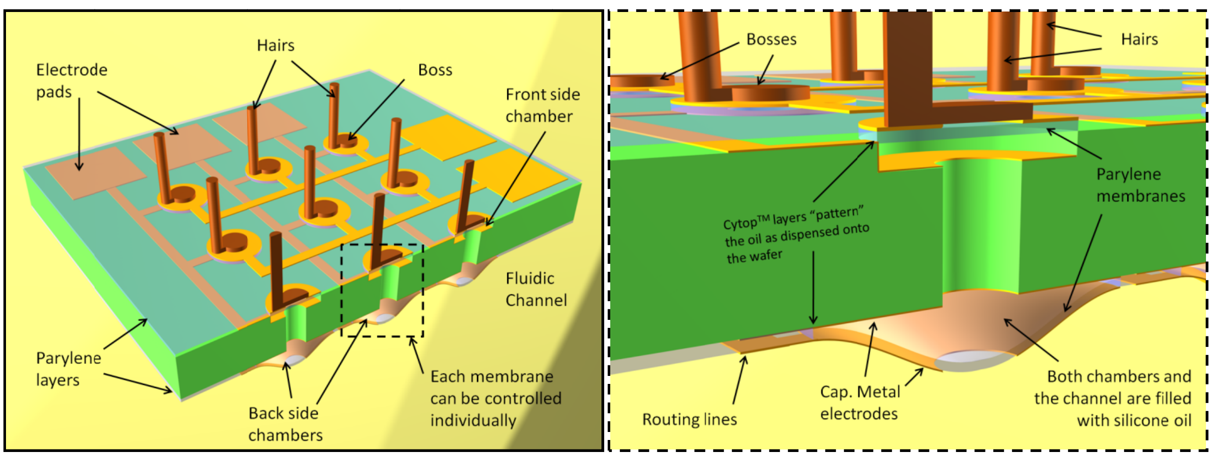

Figure 1. Micro-hydraulic structure with hairs attached on bossed membrane, after ref. 9. The base structure consists of top and bottom chambers and a pair of electrodes on the bottom membrane for either electrostatic actuation or capacitive sensing. After integration of the boss, a silicone elastomer epoxy is used to attach the tall hair over the boss.

In order to make a hair flow sensor, a hair-like post is needed to convert drag force caused by flow into pressure that is applied on the membrane. The first generation of hair flow sensor is fabricated based on the hydraulic structure shown in Figure 2 and integration of a silicon disk to form a bossed membrane[9]. The bossed membrane enables us to add appendages to the micro-hydraulic system as needed.

In the architecture shown in Figure 2, the channels connecting the chambers are shaped by deep reactive ion etching (DRIE), therefore the sidewalls are straight. As illustrated, a very narrow gap fluidic path is formed in the electrostatic gap of the backside chamber through which the liquid must flow into the channel in response to pressure exerted on the membrane. The narrower the gap is, the higher the fluidic resistance. With high fluidic resistance the sensor tends to show large rise/fall time, as shown in Figure 2. On the other hand, a narrow gap on the backside enhances the sensitivity of the device. Thus, there is a trade-off between sensitivity and response time in the straight wall architecture.

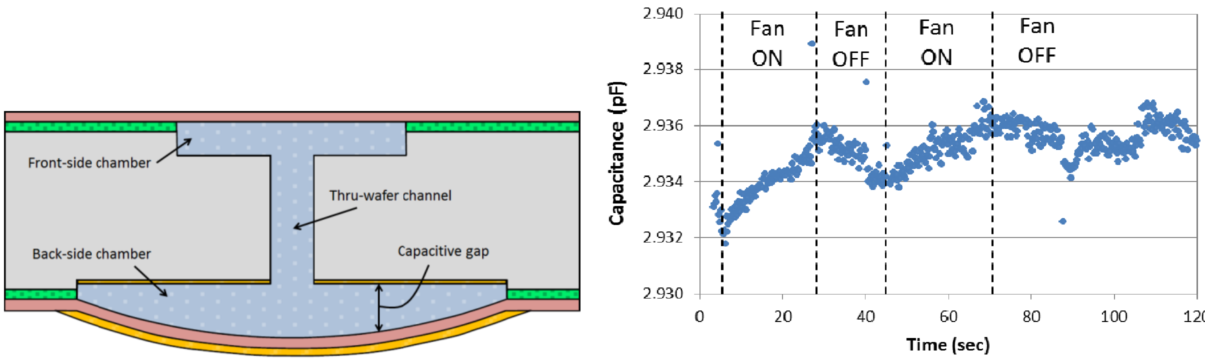

Figure 2. (left) Straight wall architecture for micro-hydraulic systems, after ref. 9. The narrow capacitive gap on the back side is filled with liquid that can form a path of high fluidic resistance. (right) Straight wall sensor response to fan cycling on and off. The response time is long.

2.2. Optimization of fluidic resistance vs. capacitance

In this section we report analysis and simulation of the dynamics of the micro-hydraulic structure to understand the dominant components dictating the time-domain behavior of the system. We show that with a fairly simple modification to the geometry of the micro-hydraulic structure, the time constant of the system can be reduced by almost three orders of magnitude while maintaining the same sensor performance.

We hypothesize that in micro-hydraulic devices the dominant delay arises from viscous fluidic flow. To verify this, we develop a 2-D multi-physics model in COMSOL that uses three linked modules: structural mechanics *(Plain Strain), Moving Mesh* and fluidics *(Incompressible Navier-Stokes)*. *Moving mesh* is used since we have observed large deflection of the top Parylene membrane[5]. First we analyze the structure in Figure 2 which is referred to as the straight wall configuration. In order to simulate the response time of the micro-hydraulic system, a step-function change in pressure is applied to the back side membrane and the deflection at the center of the front side membrane is monitored to determine the time needed for the system to reach steady-state. The depth of the front side chamber is 10 µm and that of the back side is 5 µm. The Parylene membrane thickness is set at 1 µm. The response is simulated for air, water, and silicone oil with a viscosity of 175 cSt. Silicone oil is used in the fabricated devices presented here, as well as in refs. 5 and 9. Here, air is considered to be incompressible. The results are plotted in Figure 3. For a 200-µm wide channel, silicone oil has a rise time of about 20 sec, in agreement with the results of Figure 2. The rise time for water (1 cSt) is dramatically less, 0.2 sec, and for air (0.0178 cSt) it is still less, about 2 ms. This shows that a simple model of fluid resistance which relates resistance directly to viscosity is valid for this structure, and that Poiseuille flow is the dominant component in this fluidic system[10]. Poiseuille flow relates the fluidic resistance of pipe to the fourth power of hydraulic diameter.

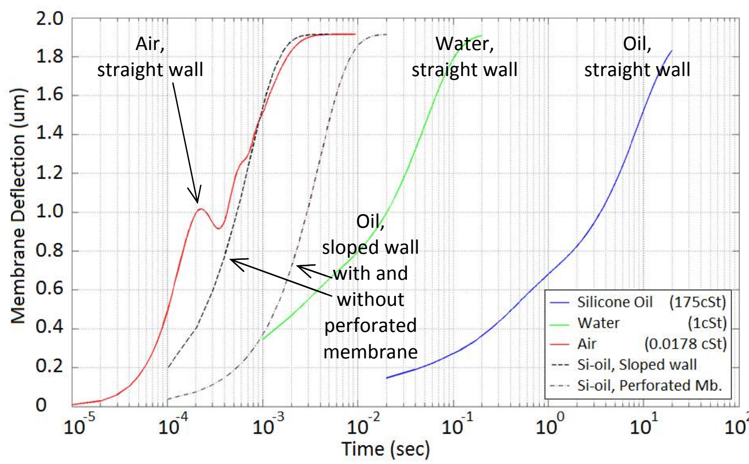

Figure 3. Simulation results comparing step response of fluids with various viscosities using straight wall geometry, and comparing silicone oil response for three architectures: straight wall, sloped wall, and sloped wall with perforated membrane. The perforated membrane 2-D model consists of 20 µm wide, 10 µm thick silicon traces separated by a spacing of 20 µm.

Since channel width plays a crucial role in response time, the best way to lower delay in the system is to widen the channel as much as possible. Also, in order to thoroughly remove any additional resistance caused by the narrow capacitive gap between the front side membrane and the front side trench, we eliminate the trench and silicon underneath and introduce a new design geometry which we refer to as “sloped wall.” The sloped walls can be fabricated with anisotropic wet etching of silicon with potassium hydroxide (KOH), tetramethylammonium hydroxide (TMAH) or EDP (ethylene diamine – pyrocatechol). In order to support the internal electrode on the backside, a perforated membrane is added. Figure 4 shows the sloped wall micro-hydraulic system with perforated membrane. The simulation results of sloped wall geometry show a tremendous improvement in the device performance. Comparing the straight wall to the sloped wall without the perforated membrane, the rise time for silicone oil is reduced by almost four orders of magnitude as shown in Figure 3. After a perforated membrane is added, there is an increase of ~5x in response time.

As discussed above, there is a compromise between fluidic resistance and capacitance. It becomes more complicated when one of the electrode plates of the capacitor is curved, as is the case for the outer membrane for which the shape is determined by liquid surface tension. However, this curved structure can be advantageous in that most of the capacitance is formed around the edge where the gap is minimal. Therefore, to improve the time response we can create a large opening in the middle of the perforated electrode, as shown in Figure 4. This dramatically lowers the fluidic resistance of the membrane but only slightly lowers the capacitance.

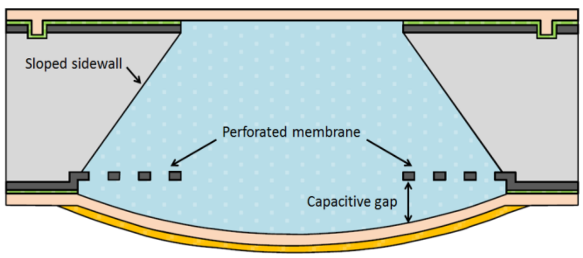

Figure 4. Sloped wall architecture with perforated membrane. A large opening is added in the middle of perforated membrane to further reduce the fluidic resistance.

To optimize the opening size, further simulations are performed. Figure 5 plots the response time of membranes with various perforation geometries calculated in sensing mode, i.e. with pressure applied to the top (smaller) side membrane and deflection measured on the (larger) backside. Wider perforation gaps and larger hole openings in the center of the membrane lead to less fluidic resistance and thus a faster response time. With perforation type 2 and a 55% opening in the center, resulting in a net 20% fill factor across the membrane, the settling time for the membrane can be reduced to 50 msec which is 400× smaller than for the straight wall geometry. It should be noted that this tremendous improvement is achieved with only a 40% reduction in total capacitance.

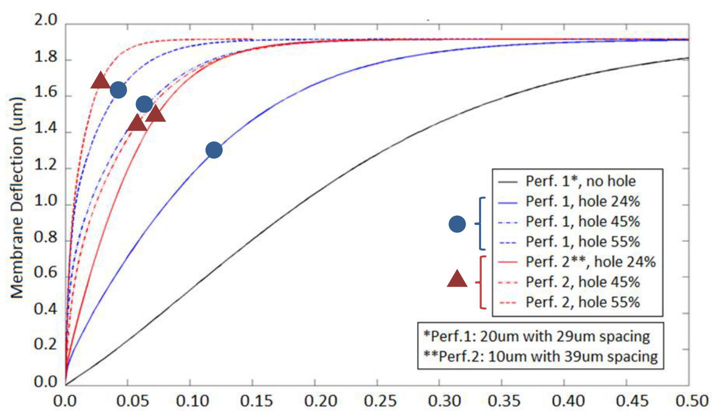

Figure 5. Comparison of response times for perforated membranes with two different perforation patterns and various center hole openings. Perforations 1 and 2 consist of 29-µm and 39-µm gaps between adjacent 20-µm and 10-µm wide silicon traces, respectively. The hole percentage is the ratio between the open hole diameter and the membrane diameter. The symbols are used solely to visually identify the lines.

2.3. Fabrication of the micro-hydraulic system

The fabrication process for sloped wall micro-hydraulic sensors is shown in Figure 6. It begins by forming DRIE trenches on the back side of the silicon wafer (step 3). To form the perforated membrane, a deep (12-µm thick) blanket boron layer is diffused on front and backside (step 2). In a second DRIE step, trenches are etched on the backside. These trenches define the perforation structure which is formed such that the EDP-etched inverted pyramids overlap. In this manner, the whole silicon bulk under the backside membrane area is etched to realize the structure shown in Figure 4. It should be noted that the deep boron doped layer will not be etched in EDP. Next, the front side DRIE trenches are etched to form the front side chamber (step 3). After this the front side is protected with 0.5 µm LPCVD oxide, and by anisotropic etching of the silicon from the back side, the floating perforated membrane and sloped walls are realized (step 4). In the next step, Cytop™, a hydrophobic polymer, is sprayed and patterned on both the front and back side of the wafer (step 5). This hydrophobic polymer helps to contain liquid droplets in Cytop™-free areas. The silicone oil is dispensed and with help of Cytop™ it is contained only in the chambers and channels (step 6). Next, the whole structure is encapsulated with Parylene. Since the silicone oil used here (1,3,5-trimethyl-1,1,3,5,5-pentaphenyltrisiloxane) has very low vapor pressure, it is not evaporated during Parylene deposition in a vacuum chamber (step 7). For the second capacitive plate, Cr/Au metal is deposited through a shadow mask onto the top of the Parylene layer (step 8). Figure 7 shows fabricated dies with arrays of micro-hydraulic structures, both before and after metal electrode deposition.

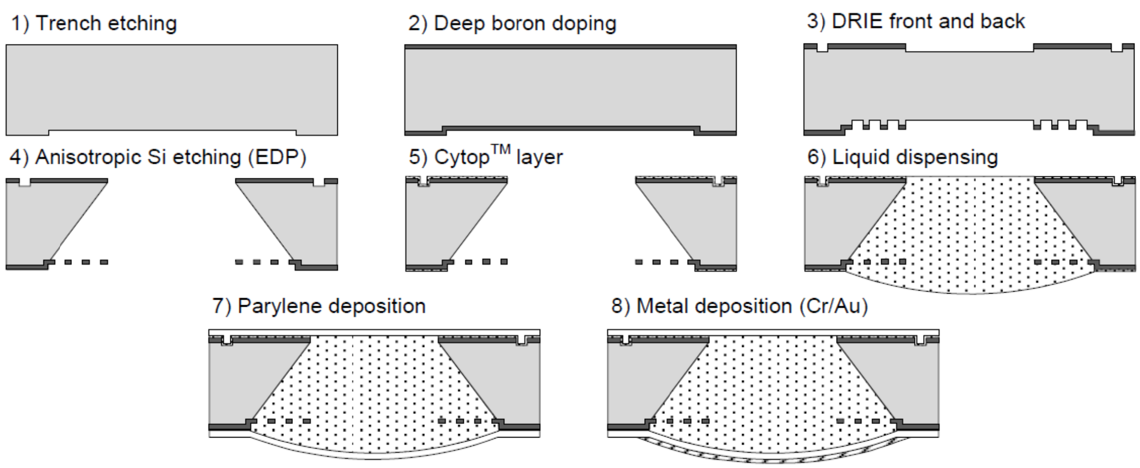

Figure 6. Sloped wall micro-hydraulic structure fabrication process with perforated membrane.

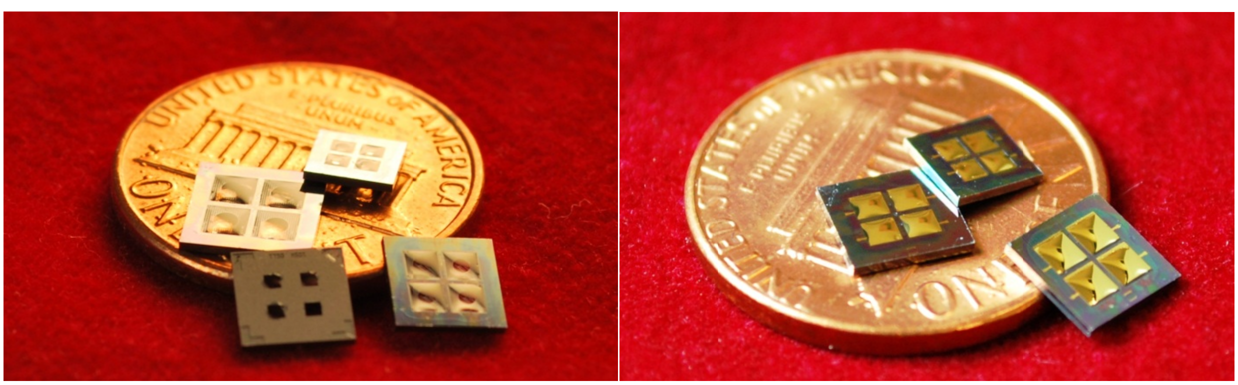

Figure 7. Fabricated arrays of micro-hydraulic structures before Cr/Au deposition (left) and after metal deposition (right).

In order to make flow sensors using this micro-hydraulic structure, hairs must be added to the front side Parylene membrane. Here, we choose as hairs prefabricated pins attached with silicone elastomer epoxy. The left side of Figure 8 shows an array of four sensors with hairs attached on the front side, and the right image shows the sensor integrated with interface circuitry.

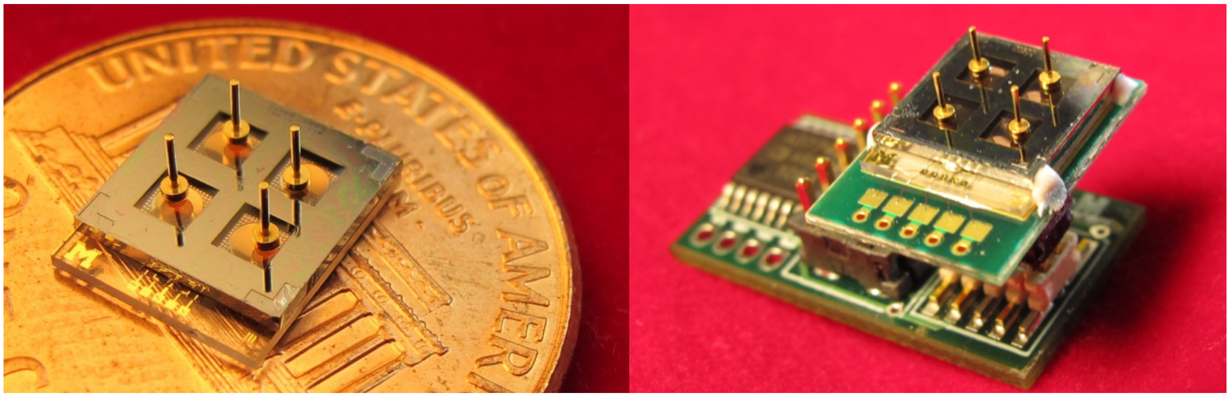

Figure 8. (Left) Hairs attached on top of a 4-cell micro-hydraulic system and (right) the same sensor integrated with interface circuitry.

3. RESULTS

In order to test the sensor, we use Analog Devices 7746 capacitance to digital converter (CDC) chip[11]. It has 21.5 ENOB with nominal resolution of 4 aF. The maximum update rate of this chip is 90.9 samples/s and the digital output is I^2C-compatible. All capacitance measurements are performed with this chip. The right side of Figure 8 shows the sensor integrated with an interface circuit on a printed circuit board (PCB) made to operate with the CDC chip. With this circuitry, the sensor can be used in applications where standalone operation is required.

3.1. Response time evaluation

We conduct two sets of experiments to evaluate the rise and fall time of the second generation air flow sensors, the results of which are shown in Figure 9. First, we test the response of the sensor to air flow from an air gun. The sensor capacitance shows quite a sharp response (lowered capacitance) upon initiation of flow and a relatively quick response as the air stream moves away from the sensor pin (capacitance value rises). Since the air flow cannot be controlled in a perfectly step-wise fashion, the flow settling time influences the measured response times. This leads us to a second experiment, in which the hair tip is mechanically touched with a non-conducting object. Here the incidence of the touch is determined by manual control, and is on therefore of order 0.1-1 s. However the touch-release time (when capacitance value rises) depends on the mechanics of the hair-hydraulic system, and thus is a more accurate measure of response time. It should be noted that the thickness of Parylene layer is chosen such that a symmetric fall/rise time of about 30 ms is achieved, for a bandwidth of about 30 Hz. Because the maximum sampling rate of AD7746 chip is of the same order as the sensor bandwidth, and due the difficulty in forming a step function of incident air flow, it is challenging to accurately quantify the response time. Therefore the true response time of the sensor may be slightly faster than that measured here.

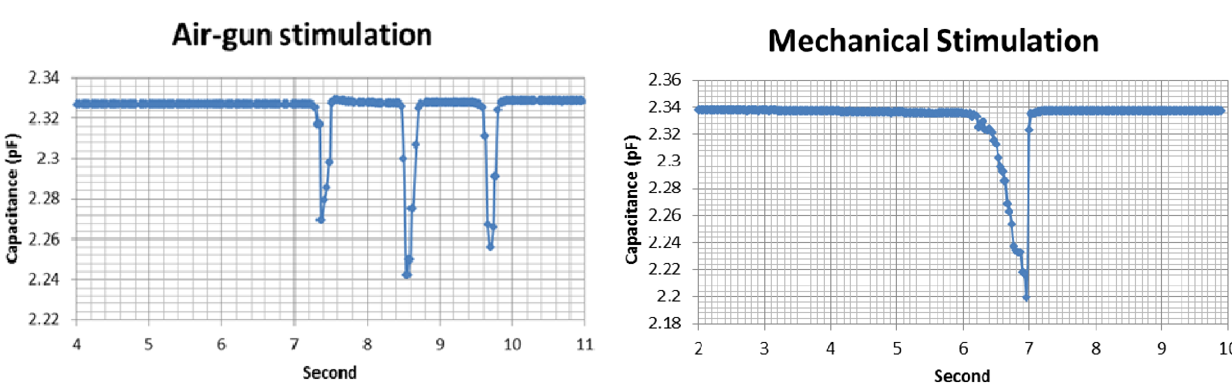

Figure 9. Response of the hair sensor to (left) an air stream blown on the sensor and (right) a mechanical touch on the hair tip. Here, the CDC sample rate is approximately 60 Hz for data point spacing of 16-17 ms.

3.2. Noise level

To measure the noise level of the system, we enclose the sensor in a box to establish a quiescent state. The measured capacitance value can fluctuate due to mechanical, thermal and circuit noise. We filter the data to eliminate a slow (< 0.1 Hz) drift in nominal capacitance. The result, plotted in Figure 10, suggests that a single-ended capacitance at the input of the CDC can be measured with accuracy of better than 80 aF.

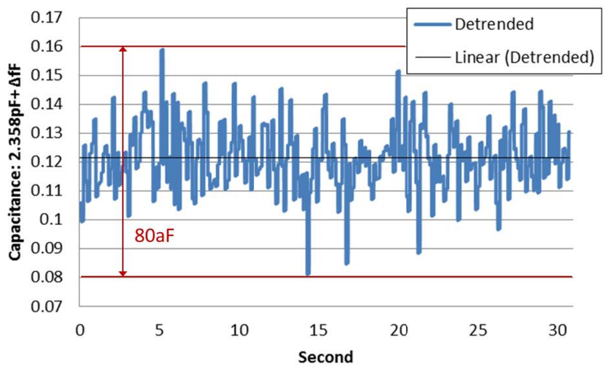

Figure 10. Noise level of the sensor under no-flow condition.

3.3. Dynamic range and resolution

We also test the sensor in a wind tunnel under steady DC flow condition. The fan speed is ramped up and the capacitance of the sensor is continuously measured. Figure 11 plots the change in capacitance as a response to change in flow speed. The sensor responds linearly to increasing flow speed from 0 to 15 m/s, the maximum air flow speed which can be generated in our wind tunnel. The sensor is very linear in this region of operation and it is likely that the actual dynamic range is larger than 15 m/s. From this measurement, the sensitivity of sensor is estimated to be 3.9 fF/(m/s). Combining this sensitivity with the minimum change in capacitance that can be reliably sensed with the sensor through CDC chip (80 aF), we calculate that air flow can be measured with resolution of slightly over 2 cm/s. Table 1 summarizes the overall performance of the sensor.

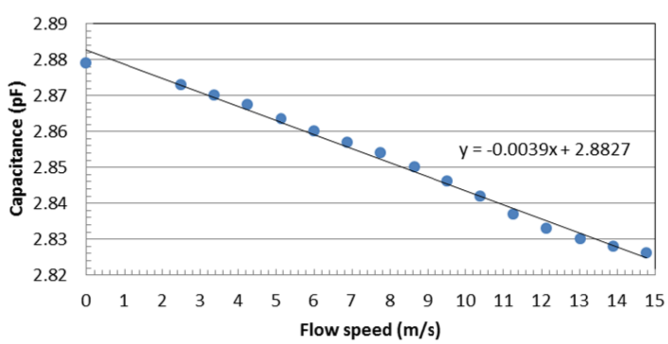

Figure 11. Capacitance change versus flow speed. The sensor response is linear throughout the tested range.

Table 1. Summary of hair flow sensor specifications

Supply	3.3 - 5 V
Range	0 – 15 m.s^{-1}
Sensitivity	3.9 fF/(m/s)
Resolution	~2.0 cm.s^{-1}
Output	I^{2}C
Response time	~30 ms
Power	3.5 mW
Weight	1.2 - 1.5 g

4. CONCLUSION

In this paper we have described hair-like air flow sensors made using a novel micro-hydraulic structure. We have analyzed the dynamics of this structure through simulation and used the results to develop a new architecture which reduces the response time of the sensor by several orders of magnitude while maintaining a wide dynamic range and high resolution. The improved hair sensors are successfully fabricated and tested. They offer a large air flow speed measurement range, high sensitivity and high bandwidth of about 30 Hz. This small, low power and high performance biomimetic air flow sensor can be integrated with autonomous platforms for situational awareness in surveillance applications or dynamic flight control by direct air flow measurement. The micro-hydraulically-amplified electrostatic sensing/actuating system shown here can also be used as a new design element in a variety of micro electromechanical devices to improve their performance.

ACKNOWLEDGMENTS

The authors thank Bing Zhang for his help in testing and characterization of the device, and the staff of the Lurie Nano-fabrication Facility (LNF) for their help in device fabrication. The LNF is a site of the National Nanotechnology Infrastructure Network (NNIN), and is funded in part through the National Science Foundation. This project is funded by the Micro Autonomous Systems & Technology (MAST) Program of the Army Research Lab (ARL) under Award Number W911NF-08-2-0004.

REFERENCES

[1] Bruinink, C. M., Jaganatharaja, R. K., de Boer, M. J., Berenschot, E., Kolster, M. L., Lammerink, T. S. J., Wiegerink, R. J., and Krijnen, G. J. M., "Advancements in technology and design of biomimetic flow-sensor arrays," Proc. IEEE Int. Conf. on Microelectromechanical Systems (MEMS), 152-155 (2009).

[2] Chen, N., Tucker, C., Engel, J. M., Yang, Y., Pandya, S. and Liu, C., "Design and characterization of artificial haircell sensor for flow sensing with ultrahigh velocity and angular sensitivity," Journal of Microelectromechanical Systems (JMEMS) 16(5), 999-1014 (2007).

[3] Wang, Y. H., Chen, C. P., Chang, C. M., Lin, C. P., Lin, C. H., Fu, L. M. and Lee, C. Y., "MEMS-based gas flow sensors," Journal of Microfluidics and Nanofluidics 6, 333-346 (2009).

[4] Kim, H. and Najafi, K., "An electrically-driven, large-deflection, high-force, micro piston hydraulic actuator array for large-scale micro-fluidic systems," Proc. IEEE Int. Conf. on Microelectromechanical Systems (MEMS), 483-486 (2009).

[5] Sadeghi, M., Kim, H. and Najafi, K., "Electrostatically driven micro-hydraulic actuator arrays," Proc. IEEE Int. Conf. on Microelectromechanical Systems (MEMS), 15-18 (2010).

[6] Sadeghi, M., Peterson, R. L., Peterson, K., Fearing, R. and Najafi, K., "Air-flow sensing on autonomous mobile platforms using micro-scale hot-wire anemometry," Proc. 27th Army Science Conference, (2010).

[7] Kaltsas, G. and Nassiopoulou, A. G., "Novel C-MOS compatible monolithic silicon gas flow sensor with porous silicon thermal isolation," Sensors and Actuators A: Physical 76(1-3), 133-138, (1999).

[8] Buchner, R., Sosna, C., Maiwald, M., Benecke, W. and Lang, W., "A high-temperature thermopile fabrication process for thermal flow sensors," Sensors and Actuators A: Physical 130-131, 262-266 (2006).

[9] Sadeghi, M. M., Peterson, R. L. and Najafi, K., "Micro-hydraulic structure for high performance bio-mimetic air flow sensor arrays," IEDM Tech. Digest, 673-676 (2011).

[10] Wilkes, J. O., [Fluid Mechanics for Chemical Engineers with Microfluidics and CFD, 2nd edition], Prentice Hall, Upper Saddle River, NJ, 312-316 (2006).

[11] Analog Devices, "AD7746 datasheet," May 2005, <http://www.analog.com/en/analog-to-digital-converters/capacitance-to-digital-converters/ad7746/products/product.html> (23 March 2012).